Enhanced dispersion in an oscillating array of harmonic traps

Joseph M. Barakat [*] and Sho C. Takatori [†]
Department of Chemical Engineering, University of California, Santa Barbara, Santa Barbara, California 93106, USA

(Received 26 September 2022; accepted 13 December 2022; published 4 January 2023)

Experiment, theory, and simulation are employed to understand the dispersion of colloidal particles in a periodic array of oscillating harmonic traps generated by optical tweezers. In the presence of trap oscillation, a nonmonotonic and anisotropic dispersion is observed. Surprisingly, the stiffest traps produce the largest dispersion at a critical frequency, and the particles diffuse significantly faster in the direction of oscillation than those undergoing passive Stokes-Einstein-Sutherland diffusion. Theoretical predictions for the effective diffusivity of the particles as a function of trap stiffness and oscillation frequency are developed using generalized Taylor dispersion theory and Brownian dynamics simulations. Both theory and simulation demonstrate excellent agreement with the experiments, and reveal a "slingshot" mechanism that predicts a significant enhancement of colloidal diffusion in dynamic external fields.

DOI: 10.1103/PhysRevE.107.014601

I. INTRODUCTION

Dispersion—the coupling between stochastic and deterministic forces that drive particle motion—is fundamental to transport in potential-energy fields. At long times and under dilute conditions, colloidal particles acted upon by an external potential move diffusively. Numerous studies have analyzed the effective diffusivity of isolated particles under static potentials [1–4], including porous media [5,6], block copolymers [7], corrugated and patterned substrates [8–10], and colloidal crystals [11,12]. Experimentally, optical tweezers provide a convenient method to trap particles in a two-dimensional (2D) periodic array of potential wells [11–15]. Although trapping in static, periodic potentials tends to hinder particle diffusion [1–3,16–19], various investigators have also reported diffusion enhancement due to broken spatial symmetry (e.g., using tilted potentials [8,9,20–22] or convective flow [13,15]).

Dynamic (i.e., time-varying) potential-energy fields produce qualitatively different dispersive phenomena. Time-oscillating optical and magnetic fields have been shown to significantly enhance particle diffusion via the "ratchet effect" [23–29]. Conceptually, this enhanced dispersion can be rationalized as a coupling between Brownian motion, a spatially modulated potential, and a time-varying, convective flow. Several studies of one-dimensional (1D) potentials report a maximum diffusivity as a function of oscillation frequency [25,28]; by comparison, 2D potentials are far less studied [26,27]. To date, the impact of potential strength and oscillation frequency on 2D dispersion has not been rigorously quantified. Consequently, the extent (and mechanism) of diffusion enhancement across a broad parameter space remains elusive. Such insight could aid in the design of systems for manipulating and controlling particles using dynamic potential-energy fields.

In this article, we combine optical tweezer experiments, Taylor dispersion theory, and Brownian dynamics simulations to investigate the dispersion of colloidal particles in a time-oscillating, 2D array of mobile potential wells. Our main objective is to systematically measure and predict the effective diffusivity across a broad range of potential strengths and oscillation frequencies, thereby identifying the conditions under which diffusion is maximally enhanced. In addition, we seek to provide simplified and intuitive predictions for the diffusivity under various limiting circumstances. Our results reveal several distinct types of 2D dispersion, including (i) random walking, (ii) trapping and hopping, and (iii) facilitated hopping or "slingshotting." In this third regime, we find that diffusion is anisotropic and maximally enhanced at a critical oscillation frequency. Somewhat surprisingly, the extent of diffusion enhancement is exaggerated by increasing the potential strength, which would ordinarily hinder diffusion under stationary (i.e., nonoscillating) conditions. We rationalize this effect based on a simplified model of a particle in an isolated potential well and, incidentally, deduce a scaling relation for the critical frequency as a function of the potential strength.

The remainder of this article is organized as follows. In Sec. II, we present a high-level overview of our experimental and theoretical methods. In Sec. III, we discuss our measurements and predictions of the particle diffusivity for stationary traps and traps oscillated at a finite frequency. Concluding remarks and suggestions for future work are then given in Sec. IV.

II. MATERIALS AND METHODS

A. Experiment

Experimentally, we use an optical tweezer (Tweez 305; Aresis) with an infrared laser (wavelength 1064 nm) to

[*] josephbarakat@ucsb.edu
[†] stakatori@ucsb.edu

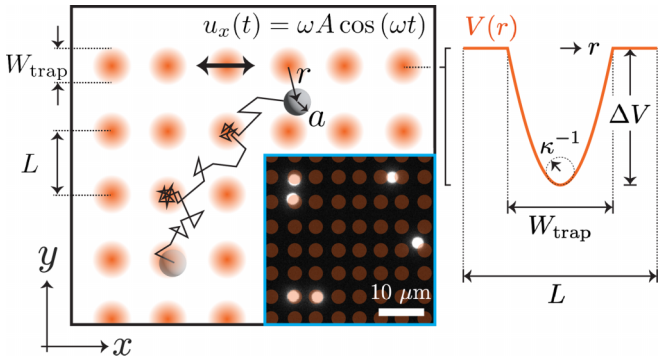

FIG. 1. Schematic of a Brownian particle diffusing in a 2D, oscillating array of harmonic traps with potential-energy field $V(\boldsymbol{r})$ and velocity $\boldsymbol{u}(t)$ given by Eqs. (1) and (2), respectively. The harmonic well has curvature κ and depth $\Delta V = \frac{1}{8}\kappa W_{\text{trap}}^2$. Inset: Experiment snapshot of radius $a = 1.25$ μm silica particles diffusing in an array of traps created by optical tweezers.

generate a 16×16 lattice of harmonic traps spaced a distance $L = 6$ μm apart along a 2D plane (see Fig. 1 for a schematic of our experimental system). The interaction of a colloidal particle with each trap is well modeled by the piecewise potential,

$$V(\boldsymbol{r}) = \begin{cases} \frac{1}{2}\kappa r^2 & \text{for } r \leqslant \frac{1}{2}W_{\text{trap}} \\ \Delta V & \text{for } r > \frac{1}{2}W_{\text{trap}}, \end{cases} \tag{1}$$

where $\boldsymbol{r}$ is the particle position relative to the trap's center, κ is the trap stiffness, W_{trap} is the trap width (≈ 3.2 μm), and $\Delta V = \frac{1}{8}\kappa W_{\text{trap}}^2$ is the potential well depth. Most optical tweezer applications employ very stiff traps (large κ) to ensure that a trapped particle does not hop out of a given potential well. However, in our experiments, we tune the laser power from 0.05 to 0.5 W to vary the trap stiffness from $\kappa = 0.5$–6 $kT/\mu\text{m}^2$, where $kT = 4.046 \times 10^{-21}$ J is the thermal energy. To study dispersion in dynamic potential-energy fields, we oscillated all traps synchronously with the sinusoidal velocity,

$$\boldsymbol{u}(t) = \hat{\boldsymbol{e}}_x \omega A \cos(\omega t), \tag{2}$$

where A is the amplitude and ω is the angular frequency. In our oscillating-trap experiments, we fix the amplitude $A = 5$ μm and vary the frequency $\omega/2\pi = 0$–66 mHz.

Silica microspheres of radius $a = 1.25$ μm (Bangs Laboratories) were fluorescently labeled by coating a supported lipid bilayer (SLB) containing a minority fraction of fluorescently tagged lipid. The lipid mixture comprised DOPC, 5% DOPS (Avanti Polar Lipids), and 0.5% DOPE-Atto 647 (ATTO-TEC GmbH). Upon depositing a dilute concentration of particles to the bottom of an imaging chamber, we observed oscillatory motion as the particles moved in and out of neighboring harmonic wells along the 2D plane. Fluorescence imaging was carried out using an inverted Nikon Ti2-Eclipse microscope (Nikon Instruments). A custom MATLAB script based on the Crocker-Grier algorithm [30–32] was used to track the particles' trajectories and measure their long-time self-diffusivity. With the trapping field switched off, we measure the Stokes-Einstein-Sutherland diffusivity $D_0 \approx 0.105$ $\mu\text{m}^2/\text{s}$, corresponding to a particle-to-wall spacing of about 0.5 μm [33]. Further details on our experimental methodology can be found in the Supplemental Material [34].

B. Theory

We apply generalized Taylor dispersion theory [5] to understand the coupling between oscillatory trap motion and colloidal diffusion. For a Brownian particle that enters an $L \times L$ cell occupied by a moving harmonic trap, the normalized probability density $g(\boldsymbol{r}, t)$ of finding the particle at a position $\boldsymbol{r}$ and time t is governed by the Smoluchowski equation,

$$\left(\frac{\partial}{\partial t} + \mathscr{L}\right) g(\boldsymbol{r}, t) = 0, \tag{3}$$

where

$$\mathscr{L}(\,\cdot\,) = \boldsymbol{u}(t) \cdot \boldsymbol{\nabla}_{\boldsymbol{r}}(\,\cdot\,) - \frac{kT}{\gamma}\nabla_{\boldsymbol{r}}^2(\,\cdot\,) - \frac{1}{\gamma}\boldsymbol{\nabla}_{\boldsymbol{r}} \cdot [(\,\cdot\,)\boldsymbol{\nabla}_{\boldsymbol{r}} V(\boldsymbol{r})] \tag{4}$$

is the time-evolution operator, $V(\boldsymbol{r})$ is the potential-energy field given by Eq. (1), $\boldsymbol{u}(t)$ is the velocity of the moving traps given by Eq. (2), and γ is the particle resistivity. The terms on the right-hand side of Eq. (4) reflect transport by convection, diffusion, and potential-energy gradients. The ratio $D_0 \equiv kT/\gamma$ defines the Stokes-Einstein-Sutherland diffusivity.

Particle density fluctuations give rise to an *effective* diffusivity that is distinct from the Stokes-Einstein-Sutherland value. The strength and orientation of these fluctuations are captured by the probability-weighted displacement field $\boldsymbol{d}(\boldsymbol{r}, t)$, which satisfies the inhomogeneous equation,

$$\left(\frac{\partial}{\partial t} + \mathscr{L}\right)\boldsymbol{d}(\boldsymbol{r}, t) = \frac{2kT}{\gamma}\boldsymbol{\nabla}_{\boldsymbol{r}} g + \frac{1}{\gamma}[g\boldsymbol{\nabla}_{\boldsymbol{r}} V - \langle g\boldsymbol{\nabla}_{\boldsymbol{r}} V\rangle\, g], \tag{5}$$

where $\langle\,\cdot\,\rangle \equiv L^{-2}\int_{L^2}(\,\cdot\,)d\boldsymbol{r}$ denotes the spatial average over an $L \times L$ cell. Clearly, the evolution of $\boldsymbol{d}$ is one-way coupled to the evolution of g through the terms on the right-hand side of Eq. (5). These terms reflect fluctuations in the probability current, which drive long-wavelength disturbances to the number density of particles. Following Brady and co-workers [35–40], it can be shown that the structure field $g(\boldsymbol{r}, t)$ is directly related to the effective drift velocity of the particle,

$$\boldsymbol{U}(t) = \boldsymbol{u}(t) - \frac{1}{\gamma}\langle g\boldsymbol{\nabla}_{\boldsymbol{r}} V\rangle(t), \tag{6}$$

while the displacement field $\boldsymbol{d}(\boldsymbol{r}, t)$ is related to the effective diffusivity tensor,

$$\boldsymbol{D}(t) = \frac{kT}{\gamma}\boldsymbol{I} + \frac{1}{\gamma}\langle \boldsymbol{d}\boldsymbol{\nabla}_{\boldsymbol{r}} V\rangle(t). \tag{7}$$

The last two expressions are the key results of the dispersion theory. They show that the enhancement (or reduction) in drift and diffusion is driven by the average particle flux down potential-energy gradients.

Equations (3) and (5) were solved numerically in an $L \times L$ cell subject to periodic boundary conditions and the normalization conditions $\langle g\rangle = 1$ and $\langle \boldsymbol{d}\rangle = \boldsymbol{0}$. Our numerical solutions were developed using the finite-element method with implicit time advancement in COMSOL MULTIPHYSICS.

The resulting g and $\boldsymbol{d}$ fields were then inserted into Eqs. (6) and (7) to compute the effective drift and diffusivity of the particle as a function of time. We validated the dispersion theory by developing Brownian dynamics simulations of 10 000 freely draining (i.e., noninteracting) particles in HOOMD-blue [41] and calculating their diffusivity from the long-time growth of their mean-squared displacements. Further details on the derivation of the relevant equations, numerical method, and simulations can be found in the Supplemental Material [34]. Below, we present the key results from the theoretical calculations and compare them against the experimental measurements.

III. RESULTS AND DISCUSSION

A. Stationary traps

When the traps are held stationary, the convective term in Eq. (4) vanishes and the particle probability distribution achieves a steady state. The absence of a time-dependent convective term in the Smoluchowski equation implies zero net drift, $\boldsymbol{U} = \boldsymbol{0}$, and an isotropic, time-independent diffusivity $\boldsymbol{D}$ with components $D_{xx} = D_{yy} = D$. Figure 2(a) shows that the scalar diffusivity D decreases monotonically with the trap stiffness κ, as reported in previous studies using one-dimensional (1D) potentials [7]. (Supplemental Material Movies S1 and S2 [34] show measured and simulated particle motion in stationary traps of varying stiffness.) For "soft" traps (i.e., potential well depths $\Delta V \ll kT$), a regular perturbation analysis admits the following expansion for the diffusivity:

$$D = \frac{kT}{\gamma}\left(1 - \frac{\langle (V - \langle V\rangle)^2\rangle}{2(kT)^2} + \frac{\langle (V - \langle V\rangle)^3\rangle + \langle \nabla_{\boldsymbol{r}}(|\nabla_{\boldsymbol{r}}\Phi|^2)\cdot\nabla_{\boldsymbol{r}}V\rangle}{4(kT)^3} + \cdots\right), \quad (8)$$

where $\Phi(\boldsymbol{r})$ satisfies $\nabla_{\boldsymbol{r}}^2\Phi(\boldsymbol{r}) = \langle V\rangle - V(\boldsymbol{r})$ and $\langle\Phi\rangle = 0$. Equation (8) indicates that the reduction in diffusivity below the Stokes-Einstein-Sutherland value is proportional to the spatial variance in the potential energy; both the first and second corrections are plotted in Fig. 2(a). In this regime, the particle trajectories appear to follow a random walk as in classical Brownian motion [see Fig. 2(b), top row].

For "stiff" traps ($\Delta V \gg kT$) held in a fixed configuration, the particles undergo activated-hopping dynamics and their diffusivity is very nearly zero. Any given particle remains trapped in a local potential well for a long time, punctuated by discrete transitions ("hops") from one well to another [see Fig. 2(b), bottom row]. Kramers' theory [16–18] suggests that the effective diffusivity is proportional to the characteristic "hopping frequency," which scales linearly with the curvature of the potential well $\kappa = \frac{1}{2}(\nabla_{\boldsymbol{r}}^2 V)|_{\boldsymbol{r}=\boldsymbol{0}}$ and exponentially with the well depth $\Delta V = \frac{1}{8}\kappa W_{\text{trap}}^2$:

$$D \propto \frac{L^2}{4\pi\gamma} e^{-\Delta V/kT}\left(\nabla_{\boldsymbol{r}}^2 V\right)\big|_{\boldsymbol{r}=\boldsymbol{0}}. \quad (9)$$

The last relationship is not exact. A constant of proportionality, which would convert Eq. (9) into an equality, depends upon the ratio W_{trap}/L between the size and spacing of the harmonic traps. For traps of diameter $W_{\text{trap}} = 3.2$ μm spaced a distance $L = 6$ μm apart, a proportionality constant of 1.5 gives quantitative agreement with the exact dispersion theory (see Fig. 2). [See the Supplemental Material [34] for the derivation of Eqs. (8) and (9).]

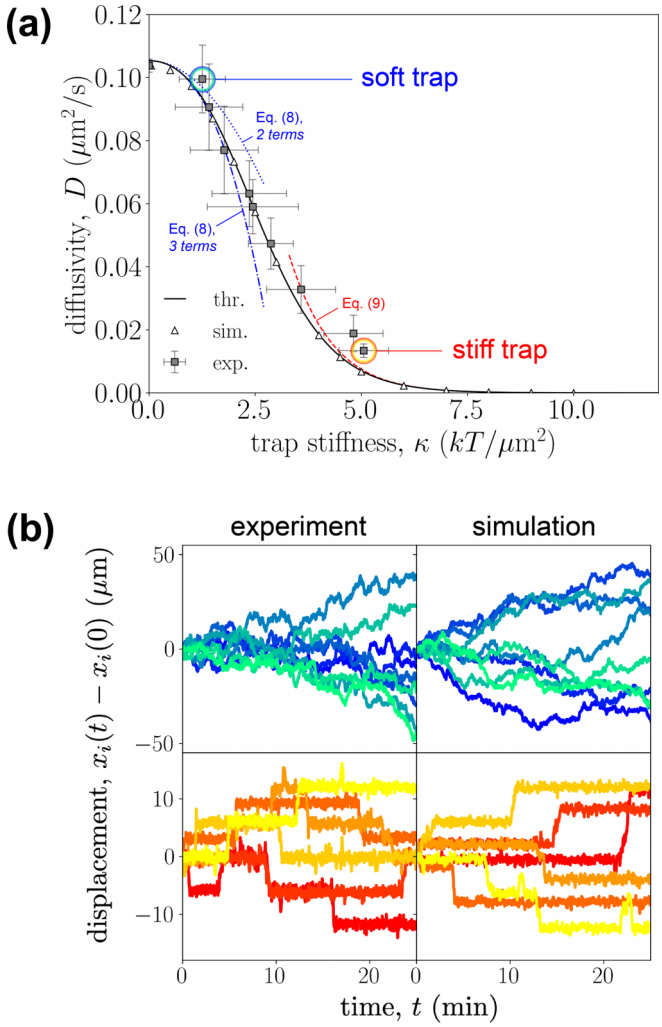

FIG. 2. Effective diffusivity D of particles in stationary traps decreases monotonically with trap stiffness κ. (a) Results from experiments (squares), Brownian dynamics simulations (triangles), Smoluchowski theory (solid line), and asymptotic limits [dashed lines; see Eqs. (8) and (9)]. A proportionality constant of 1.5 was used in Eq. (9) to fit the numerical data. (b) Particle trajectories from the experiments and simulations indicate random walks for soft traps (top row, cool colors) and activated, Kramers-like hopping for stiff traps (bottom row, warm colors). See also Supplemental Material Movies S1 and S2 [34].

B. Oscillating traps

The situation qualitatively changes when the traps are not stationary, but oscillated synchronously with the velocity prescribed by Eq. (2). After a sufficiently long time, the system achieves a periodic steady state; one is then only interested in time-averaged quantities over a periodic cycle, $\overline{(\cdot)} \equiv \lim_{\tau\to\infty}(2\pi/\omega)^{-1}\int_{\tau-\pi/\omega}^{\tau+\pi/\omega}(\cdot)dt$. It is straightforward to

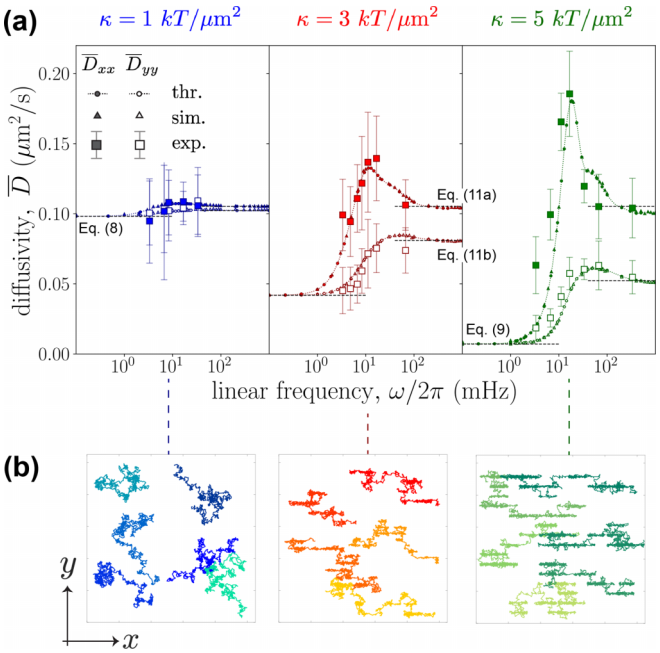

FIG. 3. Oscillating array of harmonic traps generates a nonmonotonic, anisotropic dispersion of Brownian particles. (a) Time-averaged effective diffusivities $\overline{D}_{xx}$ (filled symbols) and $\overline{D}_{yy}$ (open symbols) plotted as a function of oscillation frequency ω for different trap stiffnesses κ. Shown are results from experiments (squares), Brownian dynamics simulations (small triangles), Smoluchowski theory (small circles), and asymptotic limits [dashed lines, see Fig. 2 and Eqs. (8), (9), and (11)]. There are no fitting parameters in the theory. (b) Experimental particle trajectories at the critical frequency ω_{max}, where $\overline{D}_{xx} = \overline{D}_{xx,max}$, depict increasingly anisotropic dispersion as the trap stiffness is increased. The field of view is 100 μm × 100 μm. See also Supplemental Material Movies S3 and S4 [34] for measured and simulated particle trajectories.

show that the time-averaged drift is identically zero, $\overline{\boldsymbol{U}} = \boldsymbol{0}$, whereas the time-averaged diffusivity $\overline{\boldsymbol{D}}$ is generally nonzero and *anisotropic* ($\overline{D}_{xx} \neq \overline{D}_{yy}$) due to the existence of a preferred direction along the convection (x) axis.

Figure 3(a) illustrates the nonmonotonic dependence of the time-averaged diffusivities $\overline{D}_{xx}$ and $\overline{D}_{yy}$ with the driving frequency ω for three different trap stiffnesses $\kappa = 1$, 3, and 5 $kT/\mu m^2$ and a fixed amplitude $A = 5$ μm. The softest of these traps ($\kappa = 1\ kT/\mu m^2$) exhibits the weakest coupling between convection and potential-energy gradients: over a broad range of frequencies, diffusion remains nearly isotropic and close to the Stokes-Einstein-Sutherland limit $D_0 \approx 0.105\ \mu m^2/s$. As the trap stiffness is increased to $\kappa = 3$ and 5 $kT/\mu m^2$, the diffusivity becomes increasingly anisotropic with faster diffusion in the oscillating direction relative to the transverse direction ($\overline{D}_{xx} > \overline{D}_{yy}$). Tracking the particle trajectories, depicted in Fig. 3(b), visually confirms the anisotropic dispersion (Supplemental Material Movies S3 and S4 [34] show measured and simulated trajectories in oscillating traps of varying frequency and fixed stiffness). Both $\overline{D}_{xx}$ and $\overline{D}_{yy}$ increase to a maximum before decaying to an asymptotic plateau as ω becomes infinitely large ("ultrafast cycling"). Varying the oscillation amplitude A at fixed frequency ω reveals a similar, nonmonotonic trend (additional data provided in the Supplemental Material [34]).

The high-frequency asymptote can be understood as follows. Over a time increment much shorter than the Brownian time, a particle samples the entire potential range along the convection axis as the potential field is rapidly cycled. Therefore, the effective potential that is "felt" by the particle over one periodic cycle is approximated by averaging V over the convection axis:

$$v(y) = \frac{1}{L}\int_{-L/2}^{L/2} V(x,y)dx. \tag{10}$$

The quasisteady diffusion of a Brownian particle in a 1D potential $v(y)$ is well established [2,42], with diffusivities (derived in the Supplemental Material [34]),

$$\overline{D}_{xx} = \frac{kT}{\gamma}, \tag{11a}$$

$$\overline{D}_{yy} = \frac{kT}{\gamma}\langle e^{-v/kT}\rangle^{-1}\langle e^{v/kT}\rangle^{-1}. \tag{11b}$$

Equation (11) agrees well with the data plotted in Fig. 3(a) at the highest of frequencies. Whereas diffusion perpendicular to convection is hindered as though the particle experienced a potential-energy field given by Eq. (10), parallel diffusion is largely unaffected because the potential-energy gradients along the x direction have essentially been "smeared out." Put another way, since the time required for a Brownian particle to diffuse from one lattice site to another is much slower than the convection time ($\gamma L^2/kT \gg 2\pi/\omega$), the particle is unable to quickly respond to the rapid motion of the traps as it freely diffuses along the convection axis.

C. Maximum diffusivity

Both theory and experiment predict a maximum diffusivity that exceeds the Stokes-Einstein-Sutherland value, $\overline{D}_{xx,max} > D_0$, at a critical oscillation frequency ω_{max} (see Fig. 3). Similar maxima have been previously reported for 1D magnetic ratchets [25,28]. Figures 4(a) and 4(b) sketch the basic argument for this maximum. In a stationary system, a strongly trapped Brownian particle fluctuates with variance kT/κ about a local potential-energy minimum until a sufficiently large, thermal "kick" successfully propels the particle out of the potential well and into the interstices of the lattice [see Fig. 4(a), top, and Supplemental Material Movie S5 [34]]. Oscillatory convection displaces the particle along the x axis with amplitude $A[1 + (\kappa/\gamma\omega)^2]^{-1/2} \approx \gamma\omega A/\kappa$, bringing it towards the edge of the trap at $x = \pm\frac{1}{2}W_{trap}$ and effectively lowering the barrier to escape [see Fig. 4(b), top, and Supplemental Material Movie S6 [34]]. Consequently, the particle is never trapped for very long, but rather is catapulted between lattice sites through the motion of the harmonic traps. This "slingshot" mechanism is facilitated at a critical frequency ω_{max} for which the fluctuating particle position (with mean $\sim\gamma\omega_{max}A/\kappa$ and variance $\sim kT/\kappa$) is convected a distance $\frac{1}{2}W_{trap}$ up the potential-energy gradient. By this argument, we make the following estimate for ω_{max} (derived in the Supplemental Material [34]):

$$\omega_{max} \approx \frac{\kappa}{\gamma A}\left(\frac{1}{2}W_{trap} - \sqrt{\frac{kT}{\kappa}}\right). \tag{12}$$

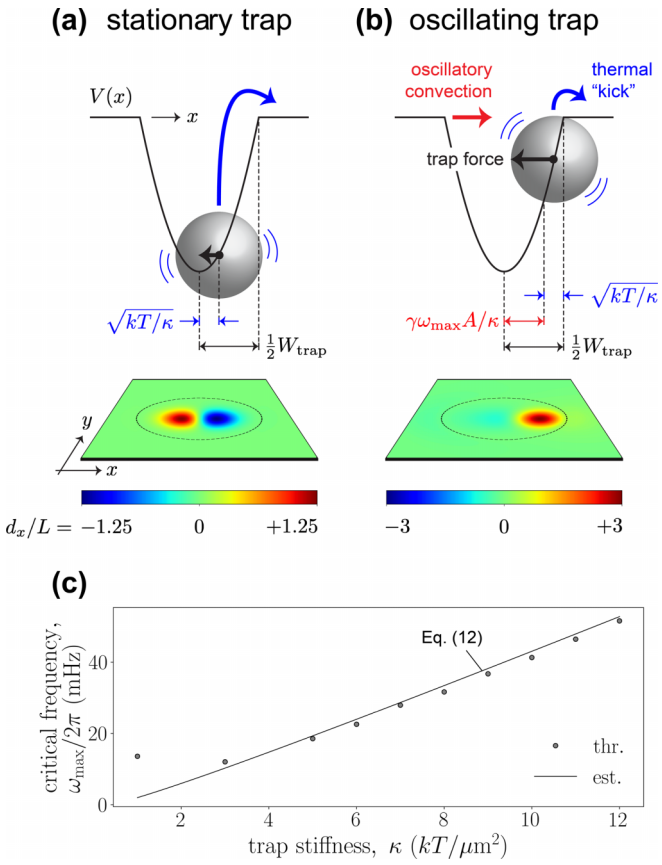

FIG. 4. "Slingshot" mechanism of enhanced dispersion in an oscillating array of harmonic traps. (a) A particle trapped in a stationary potential-energy well undergoes $O(\sqrt{kT/\kappa})$ positional fluctuations due to Brownian motion. Isocontours of the displacement field density d_x reveal a dipolar profile. (b) Oscillation at the critical frequency $\omega_{\max}$ convects the particle probability up the potential-energy gradient by an $O(\gamma\omega_{\max}A/\kappa)$ distance, effectively lowering the barrier to escape. The convected d_x field samples larger trapping forces, resulting in enhanced dispersion along the convection axis. Contour plots in (a) and (b) were generated for $\kappa = 5\ kT/\mu\text{m}^2$. See also Supplemental Material Movies S5–S7 [34] for simulated particle trajectories and displacement field densities. (c) The critical frequency $\omega_{\max}$ plotted as a function of the trap stiffness κ favorably agrees with the rough estimate given by Eq. (12).

This rough estimate qualitatively predicts the critical frequency $\omega_{\max}$ over a range of trap stiffnesses κ and quantitatively up to a relative error of about 5% above the exact calculation [Fig. 4(c)].

The enhanced dispersion can also be rationalized by plotting the two-dimensional isocontours of the displacement field density d_x with and without convection [see Figs. 4(a) and 4(b), bottom, and Supplemental Material Movie S7 [34]]. Under quiescent conditions, the d_x field is strongly localized to the center of the potential well and admits a dipolar profile. Oscillation convects the d_x field to the edge of the trap, where the potential-energy gradient $\partial V/\partial x$ is maximized. Larger trapping forces are, therefore, weighted more heavily in the force-displacement dyad $\langle d_x(\partial V/\partial x)\rangle$ that appears in the xx component of Eq. (7). This argument directly explains the maximum diffusivity $\overline{D}_{xx,\max}$ observed at the critical frequency $\omega_{\max}$.

The fact that dispersion along the convection axis increases significantly with increasing trap stiffness may be counterintuitive, given that strong harmonic traps reduce the particle diffusivity under quiescent conditions. A useful analogy is the classical Taylor-Aris dispersion of a tracer in a pressure-driven fluid flow [43,44], in which *smaller* tracer diffusivities generate stronger dispersion along the convection axis due to the coupling between longitudinal convection and transverse diffusion. This effect becomes more pronounced with increasing convection strength. In our system, the strongest dispersion occurs when convection, diffusion, and potential-energy gradients are all in play and on equal footing. If the traps are too stiff, then the particles remain confined to their wells at the mercy of thermal forces; too strong a convective velocity, and the particles are swept past the wells and only sense transverse gradients in the potential-energy landscape. The "optimal" rate of convection, for a given trap stiffness, oscillation amplitude, and particle size, is satisfactorily predicted by Eq. (12).

IV. CONCLUSIONS

We have measured and predicted the effective diffusivity of individual colloidal particles moving through a 2D oscillating array of harmonic traps in order to elucidate the influence of trapping strength and oscillation frequency. Our results revealed several distinct regimes of dispersion. Under soft trapping (i.e., weak potentials compared to kT), particles undergo random walks with a diffusivity given by Eq. (8). Stiff (but stationary) traps leading to trapping-and-hopping kinematics with Kramers-like diffusivity are given by Eq. (9). Rapid oscillation of the traps enhances diffusion parallel and perpendicular to the convection axis relative to a stationary system of equal trapping strength. The high-frequency diffusivity is given by Eq. (11) as though the particles experience an effective, 1D potential in the perpendicular direction [Eq. (10)]. Finally, we showed that the maximum diffusivity in the parallel direction occurs by a facilitated hopping or slingshotting mechanism, whereby oscillatory convection of particles up steep potential-energy gradients facilitates their escape. A scaling relation for the critical frequency at which parallel diffusion is maximally enhanced is given by Eq. (12).

Our study focused on dispersion through a 2D array of harmonic traps as a simple and tractable model for a corrugated potential-energy landscape. However, it is straightforward to draw connections to other physical systems where trapping physics and nontrivial dispersive phenomena may emerge. Examples include stick-slip diffusion and Lévy flights [45,46], active or directed motion through convection rolls [47–49], and caging in concentrated suspensions [50,51].

We end this article by providing several areas for future investigation. First, one can easily adapt our experimental system to generate other forms of time-dependent trap motion. This study focused on 1D synchronous, sinusoidal motion for simplicity; asynchronous or anharmonic kinematics will likely give rise to different couplings with the potential-energy field produced by the traps. This, in turn, could either enhance or hinder dispersion and merits further study. Second, in addition to changing the convective forcing, one could

investigate colloids with different packing densities and surface chemistries to understand how dynamic external fields impact multibody interactions (including hydrodynamic interactions) and macroscopic suspension properties. Finally, the use of self-propelled colloids would generate further couplings with the dynamic potential landscape, producing nontrivial effects that could be relevant to the field of active matter.

ACKNOWLEDGMENTS

This material is based upon work supported by the National Science Foundation (Grant No. 2150686). J.M.B. acknowledges support from the National Institutes of Health F32 Ruth L. Kirschstein National Research Service Award (Grant No. F32HL156366). S.C.T. is supported by the Packard Fellowship in Science and Engineering.

[1] P. Fulde, L. Pietronero, W. R. Schneider, and S. Strässler, Phys. Rev. Lett. **35**, 1776 (1975).
[2] R. Festa and E. G. d'Agliano, Phys. A (Amsterdam, Neth.) **90**, 229 (1978).
[3] A. K. Das, Phys. A (Amsterdam, Neth.) **98**, 528 (1979).
[4] D. L. Weaver, Phys. A (Amsterdam, Neth.) **98**, 359 (1979).
[5] H. Brenner and D. A. Edwards, *Macrotransport Processes* (Butterworth-Heinemann, Stoneham, MA, 1993).
[6] M. Mangeat, T. Guérin, and D. S. Dean, J. Chem. Phys. **152**, 234109 (2020).
[7] J.-L. Barrat and G. H. Fredrickson, Macromolecules **24**, 6378 (1991).
[8] X. G. Ma, P. Y. Lai, B. J. Ackerson, and P. Tong, Soft Matter **11**, 1182 (2015).
[9] X. G. Ma, P. Y. Lai, B. J. Ackerson, and P. Tong, Phys. Rev. E **91**, 042306 (2015).
[10] Y. Su, P.-Y. Lai, B. J. Ackerson, X. Cao, Y. Han, and P. Tong, J. Chem. Phys. **146**, 214903 (2017).
[11] K. Loudiyi and B. J. Ackerson, Phys. A (Amsterdam, Neth.) **184**, 1 (1992).
[12] C. Bechinger, Q. H. Wei, and P. Leiderer, J. Phys.: Condens. Matter **12**, A425 (2000).
[13] P. T. Korda, M. B. Taylor, and D. G. Grier, Phys. Rev. Lett. **89**, 128301 (2002).
[14] M. Pelton, K. Ladavac, and D. G. Grier, Phys. Rev. E **70**, 031108 (2004).
[15] Y. Roichman, V. Wong, and D. G. Grier, Phys. Rev. E **75**, 011407 (2007).
[16] H. A. Kramers, Physica **7**, 284 (1940).
[17] H. Brinkman, Physica **22**, 29 (1956).
[18] H. Brinkman, Physica **22**, 149 (1956).
[19] R. Zwanzig, J. Phys. Chem. **96**, 3926 (1992).
[20] S.-H. Lee and D. G. Grier, Phys. Rev. Lett. **96**, 190601 (2006).
[21] M. Evstigneev, O. Zvyagolskaya, S. Bleil, R. Eichhorn, C. Bechinger, and P. Reimann, Phys. Rev. E **77**, 041107 (2008).
[22] P. Reimann and R. Eichhorn, Phys. Rev. Lett. **101**, 180601 (2008).
[23] P. Reimann, Phys. Rep. **361**, 57 (2002).
[24] S. Bleil, P. Reimann, and C. Bechinger, Phys. Rev. E **75**, 031117 (2007).
[25] P. Tierno, P. Reimann, T. H. Johansen, and F. Sagués, Phys. Rev. Lett. **105**, 230602 (2010).
[26] S. Bianchi, R. Pruner, G. Vizsnyiczai, C. Maggi, and R. Di Leonardo, Sci. Rep. **6**, 27681 (2016).
[27] A. V. Arzola, M. Villasante-Barahona, K. Volke-Sepúlveda, P. Jákl, and P. Zemánek, Phys. Rev. Lett. **118**, 138002 (2017).
[28] R. L. Stoop, A. V. Straube, and P. Tierno, Nano Lett. **19**, 433 (2019).
[29] J. L. Abbott, A. V. Straube, D. G. Aarts, and R. P. Dullens, New J. Phys. **21**, 083027 (2019).
[30] J. C. Crocker and D. G. Grier, J. Colloid Interface Sci. **179**, 298 (1996).
[31] J. C. Crocker and E. R. Weeks, Particle tracking using IDL, software available electronically at http://www.physics.emory.edu/faculty/weeks//idl/.
[32] D. Blair and E. R. Dufresne, The MATLAB particle tracking code repository, software available electronically at https://site.physics.georgetown.edu/matlab/.
[33] J. Happel and H. Brenner, *Low Reynolds Number Hydrodynamics: With Special Applications to Particulate Media* (Martinus Nijhoff, The Hague, Netherlands, 1983), p. 327.
[34] See Supplemental Material at http://link.aps.org/supplemental/10.1103/PhysRevE.107.014601 for experiment and simulation videos, as well as a description of experimental and theoretical protocols, and which includes Refs. [52,53].
[35] J. F. Morris and J. F. Brady, J. Fluid Mech. **312**, 223 (1996).
[36] R. N. Zia and J. F. Brady, J. Fluid Mech. **658**, 188 (2010).
[37] S. C. Takatori and J. F. Brady, Soft Matter **10**, 9433 (2014).
[38] E. W. Burkholder and J. F. Brady, Phys. Rev. E **95**, 052605 (2017).
[39] E. W. Burkholder and J. F. Brady, J. Chem. Phys. **150**, 184901 (2019).
[40] Z. Peng and J. F. Brady, Phys. Rev. Fluids **5**, 073102 (2020).
[41] J. A. Anderson, J. Glaser, and S. C. Glotzer, Comput. Mater. Sci. **173**, 109363 (2020).
[42] S. Lifson and J. L. Jackson, J. Chem. Phys. **36**, 2410 (1962).
[43] R. Aris, Proc. R. Soc. London, Ser. A **235**, 67 (1956).
[44] G. I. Taylor, Proc. R. Soc. London, Ser. A **219**, 186 (1953).
[45] L. Bardotti, P. Jensen, A. Hoareau, M. Treilleux, B. Cabaud, A. Perez, and F. C. S. Aires, Surf. Sci. **367**, 276 (1996).
[46] W. D. Luedtke and U. Landman, Phys. Rev. Lett. **82**, 3835 (1999).
[47] Y. Li, L. Li, F. Marchesoni, D. Debnath, and P. K. Ghosh, Phys. Rev. Res. **2**, 013250 (2020).
[48] P. K. Ghosh, F. Marchesoni, Y. Li, and F. Nori, Phys. Chem. Chem. Phys. **23**, 11944 (2021).
[49] Y. Li, Y. Zhou, F. Marchesoni, and P. K. Ghosh, Soft Matter **18**, 4778 (2022).
[50] M. Kops-Werkhoven, C. Pathmamanoharan, A. Vrij, and H. Fijnaut, J. Chem. Phys. **77**, 5913 (1982).
[51] J. Rallison, J. Fluid Mech. **186**, 471 (1988).
[52] M. H. Bakalar, A. M. Joffe, E. M. Schmid, S. Son, M. Podolski, and D. A. Fletcher, Cell **174**, 131 (2018).
[53] S. M. Ross, *Introduction to Probability and Statistics for Engineers and Scientists*, 4th ed. (Academic, New York, 2009), Chap. 15.